Monthly Notices
of the
ROYAL ASTRONOMICAL SOCIETY

MNRAS **453,** 914–924 (2015) doi:10.1093/mnras/stv1628

# Relevance of silicate surface morphology in interstellar $H_2$ formation. Insights from quantum chemical calculations

Javier Navarro-Ruiz,[1] José Ángel Martínez-González,[1] Mariona Sodupe,[1] Piero Ugliengo[2] and Albert Rimola[1]★

[1]*Departament de Química, Universitat Autònoma de Barcelona, E-08193 Bellaterra, Spain*
[2]*Dipartimento di Chimica and NIS Centre, Università degli Studi di Torino, Via P. Giuria 7, I-10125 Torino, Italy*

Accepted 2015 July 15. Received 2015 June 2; in original form 2015 June 2

## ABSTRACT

The adsorption of H atoms and their recombination to form an $H_2$ molecule on slab models of the crystalline $Mg_2SiO_4$ forsterite (001) and (110) surfaces was studied by means of quantum mechanical calculations based on periodic density functional theory (DFT). Present results are compared with those previously reported for the most stable (010) surface, showing the relevance of the surface morphology and their stability on the $H_2$ formation. Different H chemisorption states were identified, mostly on the outermost O atoms of the surfaces. In agreement with the higher instability of the (001) and (110) surfaces, the calculated adsorption energies are larger than those for the (010) surface. Computed energy barriers for the H hopping on these surfaces are exceedingly high to occur at the very low temperatures of deep space. For the adsorption of two H atoms, the most stable complexes are those in which the H atoms form Mg-H and SiOH surface groups. From these complexes, we did not identify energetically feasible paths for $H_2$ formation through a Langmuir–Hinshelwood mechanism on the (001) surface because the initial states are more stable than the final products. However, on the (110) surface one path was found to be exoergic with very low energy barriers. This differs to that observed for the (010) surface, for which two feasible Langmuir–Hinshelwood-based channels were identified. $H_2$ formation through the Eley–Rideal mechanism was also simulated, in which an incoming H atom impinges on a pre-adsorbed H atom at the (001) and (110) surfaces in a barrierless way.

**Key words:** astrochemistry – molecular processes – ISM: clouds – ISM: molecules.

## 1 INTRODUCTION

Molecular hydrogen is the most abundant molecule in the interstellar medium (ISM; Dyson & Williams 1997; Tielens 2005). The $H_2$ molecule is extremely relevant due to its essential role in the formation of stars in diffuse clouds, and because it participates in reactions involved in the increase of the molecular complexity occurring in space. The probabilities to form $H_2$ in gas phase are negligibly small because the reaction is inefficient *via* two-body radiative association (Gould & Salpeter 1963; Latter & Black 1991), whereas in three-body association reactions the encountering of the reactants is very difficult due to the extremely low gas densities and low temperatures (Duley & Williams 1993). Therefore, the recombination of two H atoms on the surface of dust grains is thought to be the main mechanism for the formation of $H_2$ (Cazaux & Tielens 2004).

Dust is predominantly composed by carbonaceous and silicaceous materials (Herbst, Chang & Cuppen 2005). Silicate dust grains are ubiquitously present in the ISM (Draine 2003), and are mainly constituted by olivines and pyroxenes with general formula $Mg_{2x}Fe_{(2x-2)}SiO_4$ and $Mg_xFe_{(x-1)}SiO_3$ ($x = 0$–1), respectively. In the stellar outflows of dying stars silicate dust grains are formed, appearing to be partially crystalline and very Mg-rich. However, as they are exposed to various processes such as shocks and sputtering, these dust grains become amorphous (Molster & Kemper 2005) so that only a fraction of about 10 per cent is crystalline.

Several papers published in recent years studied the formation of $H_2$ on dust surfaces, both from experimental and theoretical viewpoints. A recent excellent review on this subject was published by Vidali (2013). Experimentally, the formation of $H_2$ has been studied on surfaces of water ice (Hornekær et al. 2003; Perets et al. 2005; Vidali et al. 2006, 2007), graphite (Baouche et al. 2006; Creighan, Perry & Price 2006; Hornekær et al. 2006; Islam, Latimer & Price 2007; Latimer, Islam & Price 2008), amorphous carbon (Katz et al. 1999) and crystalline (Pirronello et al. 1997; He, Frank & Vidali

★ E-mail: albert.rimola@uab.cat

2011) and amorphous silicates (Vidali et al. 2006, 2007; Perets et al. 2007; He et al. 2011), showing that in all cases $H_2$ formation from the recombination of two H atoms occurs with large efficiency. Pirronello and coworkers (Pirronello et al. 1997; Perets et al. 2007) and Vidali and coworkers (He et al. 2011) identified significant energetic differences when the formation occurs on either crystalline or amorphous silicates, the later materials presenting larger activation energies for diffusion and larger desorption energies, thereby showing the importance of the surface morphology in this reaction. Theoretical works, based on quantum mechanical methods on H adsorption and $H_2$ formation, were also published. Quantum dynamics studies addressed the $H_2$ formation on coronene clusters and C(0001) surfaces as models of carbonaceous dust grains (Meijer, Fisher & Clary 2003; Morisset et al. 2005; Bachellerie et al. 2009; Rougeau, Teillet-Billy & Sidis 2011; Casolo, Tantardini & Martinazzo 2013). By means of periodic calculations, the H adsorption on the (010) crystalline $Mg_2SiO_4$ and $Fe_2SiO_4$ surfaces (Downing et al. 2013; Garcia-Gil et al. 2013; Navarro-Ruiz et al. 2014) were exhaustively explored, showing neighbour Mg and O ions as the most favourable sites for physisorption and chemisorption, respectively. Similar results were obtained by Goumans et al. (Goumans & Bromley 2011) for the H adsorption on a ultra-small $Mg_4Si_4O_{12}$ silicate cluster (less than 15 Å in diameter). $H_2$ formation on the (010) crystalline forsterite silicate surface was studied with a QM/MM methodology (Goumans, Catlow & Brown 2009) and also by full ab initio periodic calculations (Navarro-Ruiz et al. 2014), indicating that $H_2$ formation is feasible at low ISM temperatures from both physisorbed and chemisorbed H atoms. Calculations based on a $Mg_6Si_3O_{12}$ molecular cluster (9 Å in diameter), which presents different O chemisorption sites, showed that $H_2$ formation is unfavourable when the H atoms are on the most favourable adsorption sites because the reaction is endoergic, whereas, in contrast, on the less stable sites the reaction is energetically favourable (Kerkeni & Bromley 2013).

The primary cleavage plane of forsterite ($Mg_2SiO_4$) is the (010) surface and, as reported above, the $H_2$ formation on this surface was already studied in detail by means of theoretical calculations (Goumans et al. 2009; Navarro-Ruiz et al. 2014). However, the crystal morphology of $Mg_2SiO_4$ presents other extended surfaces. It is therefore interesting to study the $H_2$ formation also on these other crystal faces, which may exhibit different chemical activity compared to the (010) surface. Present study mimics the $H_2$ formation on relatively extended interstellar grains, in which the degree of crystallinity is very high, which in turn are different to literature results of the $H_2$ formation on small forsterite clusters as they represent more closely interstellar grains in the amorphous state (Henning 2010). Comparison of the results from both cases provides a more complete scenario to elucidate the $H_2$ formation in the ISM environment by bracketing the energetic within a wider interval. In this paper, therefore, we present for the first time quantum chemical results based on periodic calculations on the H adsorption and $H_2$ formation on the (001) and (110) crystalline surfaces, which are less stable than the (010) (Watson et al. 1997; de Leeuw et al. 2000; Bruno et al. 2014). Present study will allow us to compare with the results previously obtained for the (010) surface (Navarro-Ruiz et al. 2014), and analyse the relevance of the surface morphology on this fundamental reaction.

## 2 METHODS

Crystalline periodic slab models for the non-polar (001) and (110) forsterite surfaces were derived from appropriate geometrical cut of the forsterite crystal bulk structure (*Pbnm* space symmetry). Fig. 1 shows the resulting slab models. They contain 56 atoms per unit cell with a thickness of 11.714 and 8.128 Å, respectively. The outermost $Mg^{2+}$ cations of the (001) and (110) surfaces are coordinatively unsaturated being bounded to four and three O atoms, respectively. In the bulk crystal structure, $Mg^{2+}$ cations are octahedrally coordinated.

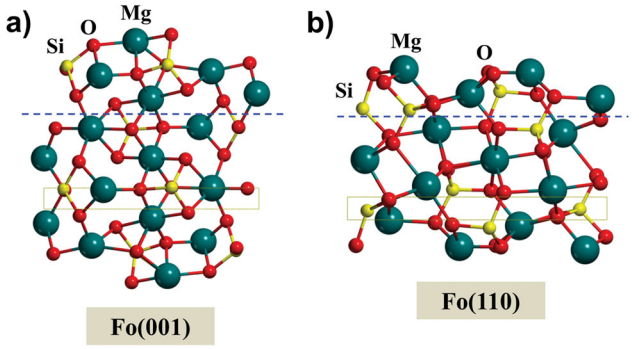


**Figure 1.** Lateral views of the crystalline (001) (a) and (110) (b) $Mg_2SiO_4$ surface models. Unit cells are highlighted in yellow, and atoms above the blue dashed lines are those included in the frequency calculations.

All calculations were carried out using the periodic ab initio code CRYSTAL09 (Dovesi et al. 2005, 2009). All the self-consistent field (SCF) calculations and geometry optimizations were performed in *P1* group symmetry using the B3LYP-D2* density functional method, which includes an empirical a posteriori correction term proposed by Grimme (2006) to account for dispersion forces [missed in the pure B3LYP (Becke 1993) method]. The original parameterization (D2) was modified for extended systems (D2*) (Civalleri et al. 2008), to provide accurate results for the calculations of cohesive energies of molecular crystals and of adsorption processes within a periodic treatment (Ugliengo & Damin 2002; Civalleri et al. 2010; Boese & Sauer 2013). Transition state (TS) structures were localized using the distinguished reaction coordinate technique as implemented in CRYSTAL09, which has proved to be robust and efficient for the characterization of the proton jump of dry and hydrated acidic zeolites (Rimola et al. 2010). For all TS structures, we checked that only one imaginary frequency resulted by the Hessian matrix diagonalization. For all calculations involving one H adsorption we adopted an unrestricted formalism, whereas for dihydrogen adsorption the starting guess was open shell broken symmetry but collapsed to the closed shell system. Net charges and electron spin densities on the atoms were derived from the Mulliken population analysis.

For the atoms belonging to the forsterite surfaces, we adopted two different Gaussian basis sets: B1 and B2. B1 is an all-electron basis set, with the following contractions: (8s)–(831sp)–(1d) for Si; (6s)–(31sp)–(1d) for O; (6s)–(631sp)–(1d) for the external layer Mg ions at the top and bottom of the slabs (standard 6–31G(d,p) Pople basis set); and (8s)–(61sp)–(1d) for the remaining Mg atoms. B2 is and all-electron basis set described by the larger contractions: (8s)–(6311sp)–(1d) for Si; (8s)–(411sp)–(1d) for O; (631111s)–(42111p)–(1d) for the top-layer Mg ions at the top and bottom of the slabs (standard 6–311G(d,p) Pople basis set) and (8s)–(511sp)–(1d) for the remaining Mg ions. Hydrogen atoms is described, for all calculations, with the TZP basis set from Ahlrichs and coworkers (Schafer, Horn & Ahlrichs 1992). We used basis set B1 for geometry optimizations and, to save computer time, basis set B2 for single point energy calculations at the B1 geometries (hereafter referred

to as B2//B1). In a previous work (Navarro-Ruiz et al. 2014), we showed that B2//B1 energy values are almost indistinguishable from those at B2//B2 level.

We set the shrinking factor of the reciprocal space net, defining the mesh of $k$ points in the irreducible Brillouin zone, to 5 and 20 for B1 and B2//B1 calculations, respectively, requiring the diagonalization of the Hamiltonian matrix in three and six $k$ points, respectively. The accuracy of both Coulomb and exchange series was set to values of overlap integrals of $10^{-6}$ and $10^{-16}$. A pruned (75, 974) grid (CRYSTAL09 keyword XLGRID) has been used for the Gauss–Legendre and Lebedev quadrature schemes in the evaluation of functionals. The condition to achieve SCF convergence between two subsequent cycles was set to $10^{-7}$ Hartree. For the modelling of the bare surfaces, relaxations of both the internal atomic coordinates and the unit cell parameters were carried out, whereas for hydrogen adsorption and recombination only the internal atomic coordinates were optimized while the unit cell parameters were kept fixed to the optimized values of the bare surfaces. The geometry optimization was performed by means of analytical energy gradients (Doll 2001) using a quasi-Newton algorithm in which the quadratic step (the Broyden-Fletcher-Goldfarb-Shanno Hessian updating scheme, BFGS) is combined with a linear one as proposed by Schlegel (Civalleri et al. 2001).

H atom adsorption and recombination was only considered on the top surface of the slabs, since this greatly simplifies the localization of TS structures. We are conscious that this approach breaks the symmetry of the system with, nevertheless, a negligible effect on the energy profiles. The energy of adsorption ($\Delta E$) for a single H atom on the forsterite surface per unit cell is

$$\Delta E = E_{\rm SH} - (E_{\rm S} + E_{\rm H}), \tag{1}$$

where $E_{\rm SH}$ is the energy of the relaxed unitary cell containing the surface structure S in interaction with the H atom, $E_{\rm S}$ is the energy of the relaxed unitary cell of the free surface slab and $E_{\rm H}$ is the energy of the free H atom. To facilitate the comparison with other computed and experimental results of astrochemical interest adsorption/desorption energies are shown in units of kcal mol$^{-1}$, meV and K.

CRYSTAL09 computes the zero-point energy (ZPE) corrections and the thermodynamic quantities by the standard statistical thermodynamics formulas based on partition functions derived from the harmonic oscillator approximations which are used to correct the adsorption energy values by temperature effects. Vibrational frequencies of the considered systems were computed at the $\Gamma$ point (point $k = 0$ in the first Brillouin zone, called central zone) within the harmonic approximation by obtaining the eigenvalues from diagonalization of the mass-weighted Hessian matrix. This dynamical matrix was obtained by numerical differentiation (central-difference formula) of the analytical first-energy derivatives, calculated at the geometries obtained by varying, in turn, each of the $3N$ equilibrium nuclear coordinates by a small amount $u = 0.003$ Å. For more detailed discussion on the computational conditions and other numerical aspects related to calculation of the vibrational frequencies at the $\Gamma$ point see (Pascale et al. 2004). For the considered systems in this work, building up the full mass-weighted Hessian matrix would have been very expensive because $N$ atoms in the unit cell would imply performing $3N + 1$ energy *plus* gradient calculations in the central-difference formula. To save computer time, only a portion of the dynamical matrix was computed by considering the displacements of a subset of atoms; i.e. the H atoms and the first- and second-layered atoms of the top surface only (see Fig. 1 for a detailed view of the included atoms).

Tunnelling effects can play a significant role in the studied processes considering the very low temperatures and the fact that they involve H atoms. The importance of tunnelling effects primarily depends on the curvature of the barrier to hydrogen transfer, which is controlled by the transition vibrational frequency and, to a lower degree, on the height of the barrier. We have determined the tunnelling crossover temperature ($T_{\rm X}$), below which tunnelling becomes dominant and above which tunnelling becomes negligible, which can be calculated using the formula by Fermann & Auerbach (2000):

$$T_{\rm X} = \frac{h\nu^{\neq}\Delta U_0^{\neq}/k_{\rm B}}{2\pi\,\Delta U_0^{\neq} - h\nu^{\neq}\ln 2}, \tag{2}$$

where $\nu^{\neq}$ is the frequency of the transition normal mode, $h$ is the Planck constant, $\Delta U_0^{\neq}$ is the ZPE-corrected energy barrier and $k_{\rm B}$ is the Boltzmann constant. Moreover, we calculated rate constants in a semi-classical way ($k^{\rm SC\text{-}TST}$), in which tunnelling contributions are accounted for by introducing the transmission coefficient (($\Gamma(T)$) developed by Fermann & Auerbach (2000) into the classical rate constant ($k^{\rm TST}$) adopting the Eyring equation from the TS theory, i.e.

$$k^{\rm SC-TST} = k^{\rm TST} \times \Gamma\,(T) \tag{3}$$

$$\Gamma\,(T) = {\rm e}^{\Delta U_0^{\neq}/k_{\rm B}T}\,{\rm e}^{-2\pi\,\Delta U_0^{\neq}/h\nu^{\neq}}\left(1 + \frac{2\pi k_{\rm B}T}{h\nu^{\neq}}\right) \tag{4}$$

$$k^{\rm TST} = \frac{k_{\rm B}T}{h}{\rm e}^{\left(-\frac{\Delta G^{\neq}}{RT}\right)}, \tag{5}$$

where $\Delta G^{\neq}$ is the free energy barrier calculated at the temperature $T$.

## 3 RESULTS

This section is organized as follows. First, the theoretical characterization of the crystalline (001) and (110) surfaces of forsterite [henceforth referred to as Fo(001) and Fo(110), respectively] is presented, in particular some structure and energy-related features. Then, results on the H interactions with Fo(001) and Fo(110) and the $H_2$ formation on these two surfaces are shown in the subsequent sections.

### 3.1 Theoretical characterization of Fo(001) and Fo(110)

The structure of the optimized Fo(001) is shown in Fig. 1(a). Surface relaxation brings about significant changes compared to the initial slab cut, as the outermost Mg atoms move towards the internal structure by 0.4 Å, making the surface more compact, and displace laterally by 0.6 Å to coordinate to four O atoms adopting a seesaw shape. The optimized surface exhibits, as local surface defects, a tetracoordinated Mg atom and an O corner atom. Fig. 1(b) shows the optimized slab model for the Fo(110) case. Surface reconstruction from the initial slab cut does not result in significant structural changes and the optimized model present two outermost Mg atoms that are tricoordinated by O atoms in a pyramidal geometry.

The calculated equilibrium interatomic distances of Fo(001) and Fo(110) surfaces, the optimized cell parameters and the calculated surface energies are given in Table 1. In general, our structural parameters are in agreement with those of Watson et al. (1997), in which the atomistic simulations of these surfaces were performed using the THB1 interatomic potential. The internal Si−O distances are very similar with respect to the bulk values, the maximum variation belonging to Fo(001) (between 0.6 and 1.3 per cent). Larger

**Table 1.** Si–O and Mg–O range of the B3LYP-D2*-optimized bond distances of the Fo(001) and Fo(110) slab models. The values corresponding to bulk forsterite (Fo bulk) are also included. Bare values correspond to distances involving atoms present in the internal structure of the surfaces, whereas values in italics correspond to distances involving atoms present at the outermost positions of the edge-layers. B3LYP-D2*-optimized cell parameters and surface energies of the different slab models.

| | Fo(001) | Fo(110) | Fo bulk |
|---|---|---|---|
| Si–O (Å) | 1.647–1.678 | 1.631–1.670 | 1.628–1.667 |
| | *1.610–1.665* | *1.597–1.705* | |
| Mg–O (Å) | 1.996–2.284 | 1.986–2.366 | 2.073–2.222 |
| | *1.995–2.052* | *1.856–2.144* | |
| *a* (Å) | 4.838 | 5.831 | |
| *b* (Å) | 9.960 | 11.537 | |
| *ab* (degrees) | 92.48 | 91.46 | |
| Area (Å$^2$) | 48.15 | 67.25 | |
| $E_{surf}$ (J m$^{-2}$) | 1.673 | 1.788 | |

variations, although not dramatic, are observed for the internal Mg–O distances, the maximum one corresponding to Fo(110) (between 4.2 and 6.5 per cent). These results demonstrate that no important changes are appreciable in the innermost positions of the surfaces during the surface reconstruction. In contrast, more significant variations are observed for those distances involving the outermost atoms. For both slab models, the Mg–O lengths decrease (variations of about 5.8–7.7 per cent in Fo(001) and 3.5–10 per cent in Fo(110)) because they are undercoordinated, whereas the changes of the Si–O distances are less pronounced (about 2.3 per cent). The optimized lattice parameters of Fo(001) are very similar to those previously reported (Watson et al. 1997; de Leeuw et al. 2000; Bruno et al. 2014) (largest variation of 0.04 per cent), whereas for Fo(110) the variations are more accentuated (about 1.8 per cent), which is attributed to the inclusion of dispersion (D2*) in the present study, since the results are converged with respect to the thickness of the slab. Despite the relatively small slab thickness, the calculated surface energies ($E_{surf}$) of Fo(001) and Fo(110) are 1.67 and 1.79 Jm$^{-2}$, in line with literature values. For the most stable (010) case, we computed a surface energy of 1.16 Jm$^{-2}$, which confirms the same ranking of surface stability predicted in previous works (Watson et al. 1997; de Leeuw et al. 2000; Bruno et al. 2014). Finally, net Mg and O net charges obtained by a Mulliken population analysis confirm the ionic character of the surface as they are +0.82|e| and −1.01|e| for the Fo(001), and +0.97|e| and −1.01|e| for the Fo(110), respectively.

### 3.2 H adsorption and $H_2$ formation on forsterite surfaces

The formation of $H_2$ molecules on forsterite surfaces *via* Langmuir–Hinshelwood (Langmuir 1922; Hinshelwood 1930), Eley–Rideal (Eley & Rideal 1940; Eley 1941) or 'hot atom' (Harris & Kasemo 1981) mechanisms always involves, as a first step, the adsorption of at least one of the reactants on the substrate. Regardless of the mechanism, studying the features relative to the adsorption of hydrogen atom is an essential requirement to understand the subsequent recombination. Therefore, we first address in detail the H adsorption on Fo(001) and Fo(110). Moreover, as the Langmuir–Hinshelwood mechanism is probably dominant because of the very low H flux regime in the ISM, we studied the energy profiles related to the H diffusion between different adsorption sites. Then, results concerning the adsorption of a second H atom and the $H_2$ formation will be reported.

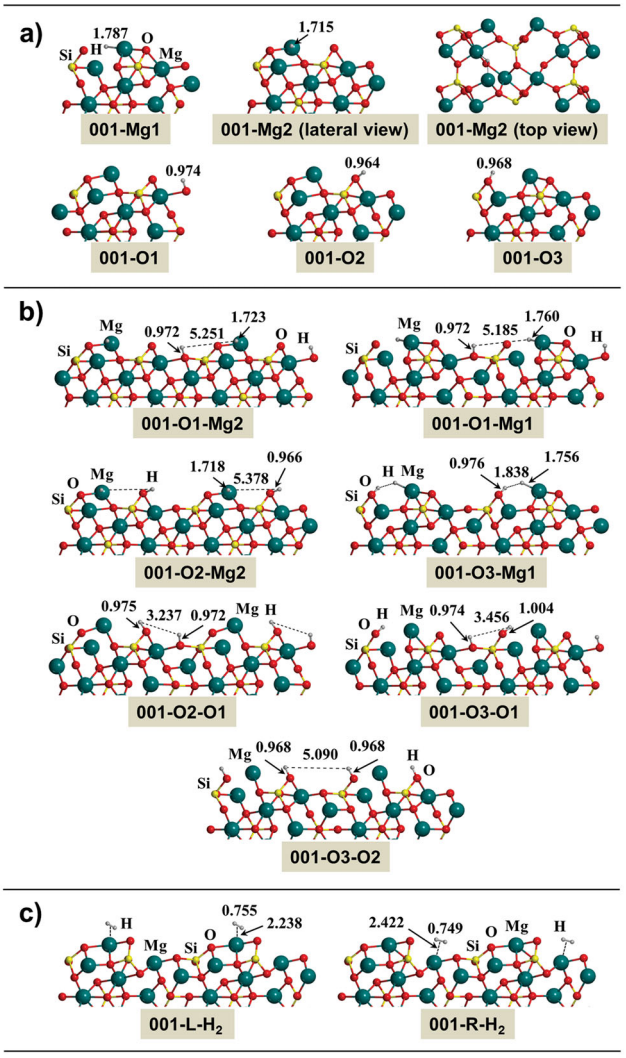


**Figure 2.** B3LYP-D2* optimized geometries of the different complexes resulting from the adsorption of (a) one H atom (001–Mg1, 001–Mg2, 001–O1, 001–O2 and 001–O3), (b) two H atoms (001–O1–Mg2, 001–O1-Mg1, 001–O2-Mg2, 001–O3-Mg1, 001–O2-O1, 001–O3-O1 and 001–O3-O2) and (c) $H_2$ (001–L-$H_2$ and 001–R-$H_2$) on the (001) $Mg_2SiO_4$ surface. Bond distances in Å (the unit cell has been doubled to highlight the H–H interactions).

#### 3.2.1 *(001) forsterite surface*

*Adsorption of one H atom.* Fig. 2(a) shows the B3LYP-D2*/B1 optimized complexes for the adsorption of one H atom on Fo(001), and Table 2 reports the computed adsorption energies calculated at B2//B1 theory level. Energy values calculated with both B1 and B2//B1 basis sets for all the processes described in this work are reported in the electronic supplementary information (ESI). We characterized five different H/Fo complexes: two in which the H atom is interacting with the uppermost Mg atom (001–Mg1 and 001–Mg2), and three in which the H atom interacts with the most exposed O atoms (001–O1, 001–O2 and 001–O3), thus forming a surface silanol (SiOH) group. It is worth mentioning that in 001–Mg1 and 001–O3, the outermost Mg atom displaces laterally giving rise to a different surface atomic distribution in the edge-layers.

According to the calculated adsorption energies (see Table 2), the most stable adduct is 001–O3. The largest adsorption energies

**Table 2.** B3LYP-D2* reaction energies calculated at the B3LYP-D2*/B2 // B3LYP-D2*/B1 theory level on Fo(001) for: (i) the first H adsorption processes to form the 001–Mg1, 001–Mg2, 001–O1, 001–O2 and 001–O3 adducts; (ii) the global H adsorption processes to form the 001–O1-Mg2, 001–O1-Mg1, 001–O2-Mg2, 001–O3-Mg1, 001–O2-O1, 001–O3-O1, 001–O3-O2, 001–L-$H_2$ and 001–R-$H_2$ complexes and (iii) the $H_2$ formation from the 2H/Fo(001) complexes. The zero-energy reference is the Fo(001) + H asymptote. Uncorrected ($\Delta E$) and ZPE-corrected ($\Delta U_0$) adsorption energy. Bare values in kcal mol$^{-1}$, in parenthesis in meV, in brackets in K.

| Reaction | $\Delta E$ | | | $\Delta U_0$ | | |
|---|---|---|---|---|---|---|
| Fo(001) + H → 001–Mg1 | − 14.1 | (−612) | [−7097] | − 11.1 | (−483) | [−5599] |
| Fo(001) + H → 001–Mg2 | − 6.7 | (−289) | [−3357] | − 2.7 | (−117) | [−1354] |
| Fo(001) + H → 001–O1 | − 40.1 | (−1739) | [−20 184] | − 33.0 | (−1432) | [−16 615] |
| Fo(001) + H → 001–O2 | − 51.5 | (−2234) | [−25 921] | − 44.5 | (−1930) | [−22 402] |
| Fo(001) + H → 001–O3 | − 55.3 | (−2396) | [−27 808] | − 48.4 | (−2098) | [−24 342] |
| Fo(001) + 2H → 001–O1-Mg2 | − 122.7 | (−5320) | [−61 742] | − 110.9 | (−4808) | [−55 796] |
| Fo(001) + 2H → 001–O1-Mg1 | − 116.2 | (−5037) | [−58 455] | − 104.9 | (−4548) | [−52 782] |
| Fo(001) + 2H → 001–O2-Mg2 | − 131.6 | (−5708) | [−66 235] | − 120.0 | (−5204) | [−60 393] |
| Fo(001) + 2H → 001–O3-Mg1 | − 137.9 | (−5981) | [−69 409] | − 126.8 | (−5501) | [−63 833] |
| Fo(001) + 2H → 001–O2-O1 | − 76.5 | (−3318) | [−38 504] | − 62.9 | (−2728) | [−31 655] |
| Fo(001) + 2H → 001–O3-O1 | − 70.6 | (−3060) | [−35 510] | − 57.8 | (−2505) | [−29 074] |
| Fo(001) + 2H → 001–O3-O2 | − 84.3 | (−3657) | [−42 441] | − 71.1 | (−3085) | [−35 799] |
| Fo(001) + 2H → 001–L-$H_2$ | − 116.2 | (−5040) | [−58 485] | − 107.2 | (−4649) | [−53 954] |
| Fo(001) + 2H → 001–R-$H_2$ | − 114.4 | (−4960) | [−57 557] | − 105.7 | (−4583) | [−53 179] |
| 001–O1-Mg2 → 001–L-$H_2$ | 6.5 | (280) | [3257] | 3.7 | (159) | [1842] |
| 001–O1-Mg1 → 001–L-$H_2$ | 0.0 | (−3) | [−30] | − 2.3 | (−101) | [−1172] |
| 001–O2-Mg2 → 001–L-$H_2$ | 15.4 | (668) | [7750] | 12.8 | (555) | [6439] |
| 001–O3-Mg1 → 001–L-$H_2$ | 21.7 | (941) | [10 924] | 19.6 | (852) | [9879] |
| 001–O2-O1 → 001–L-$H_2$ | − 39.7 | (−1722) | [−19 981] | − 44.3 | (−1921) | [−22 299] |
| 001–O3-O1 → 001–L-$H_2$ | − 45.6 | (−1980) | [−22 975] | − 49.4 | (−2144) | [−24 880] |
| 001–O3-O2 → 001–L-$H_2$ | − 31.9 | (1383) | [−16 044] | − 36.1 | (−1564) | [−18 155] |

(between −48 and −33 kcal mol$^{-1}$, $\Delta U_0$ values of Table 2) are exhibited by the O-interacting systems, followed by 001–Mg1 (−11.1 kcal mol$^{-1}$) and by 001–Mg2 (−2.7 kcal mol$^{-1}$). The Mulliken spin density for 001–Mg1 and 001–Mg2 is almost entirely localized on the nearest O atoms (+0.92|e| and +0.94|e|, respectively), whereas for 001–O1, 001–O2 and 001–O3 it is on the neighbouring outermost Mg atom (+0.93|e|, +0.93|e| and +0.91|e|, respectively), indicating an $H^+$ character of the H adatom. ESI includes the whole set of net Mulliken charges and spin densities for all considered adducts. Spin density values, as well as the O–H and H-Mg distances, indicate that all adducts are chemisorbed states. This is in contrast to that observed for Fo(010) (Navarro-Ruiz et al. 2014), for which several physisorbed states with spin density located at the H atom and O···H and Mg···H distances larger than 2.0 Å were localized.

Fig. 3(a) shows the energy profile corresponding to the 001–Mg2 → 001–Mg1 → 001–O3 path (namely, from the less to the most stable adsorption sites). The first step involves the breaking of the Mg–O simultaneously associated with a rearrangement of the H atom on the Mg atom. The second step consists of an H jump from the Mg atom to the O atom. Fig. 3(b) shows the energy profile for the H jumps that connect the different chemisorption states along the 001–O2 → 001–O1 → 001–O3 path. For this case, all jumps involve a synchronous O–H breaking/formation on the surface. The calculated energy barriers ($\Delta {U_0}^{\neq}$) of all these processes are significantly high (between 13.7 and 23.8 kcal mol$^{-1}$), due to the cleavage of chemical bonds and thus, these processes appear to be kinetically hindered at low temperatures. This means that, upon H adsorption, the systems will not evolve towards the most stable adsorption state and, accordingly, all the described adsorption states, if formed, are metastable in relation to $H_2$ formation.

*Adsorption of a second H atom.* To simulate the formation of the $H_2$ molecule on the (001) forsterite surface through a Langmuir–Hinshelwood mechanism, we also studied the adsorption of a second H atom on the 001–Mg1, 001–Mg2, 001–O1, 001–O2 and 001–O3 adducts. We considered a total of 10 initial guess adducts by combining the different H/Fo complexes: (i) three derived from the combination of 001–Mg1 with the second H atom adsorbed on the three available O atoms (i.e. 001–O1-Mg1, 001–O2-Mg1 and 001–O3-Mg1); (ii) three derived from the combination of 001–Mg2 with the O atoms (i.e. 001–O1-Mg2, 001–O2-Mg2 and 001–O3-Mg2); (iii) three derived from the combination of the O-interacting adducts (i.e. 001–O2-O1, 001–O3-O1, 001–O3-O2); and (iv) one derived from the combination of 001–Mg1 and 001–Mg2 (i.e. 001–Mg1-Mg2). Geometry optimization of all these starting structures collapsed into seven different complexes. Fig. 2(b) shows the B3LYP-D2* optimized structures of these adducts and Table 2 the calculated total adsorption energies, that is, the reaction energy of Fo(001) + 2H → 2H/Fo(001). ESI reports the adsorption energies of the second H atom from the H/Fo(001) complexes (i.e. the reaction energy of H/Fo(001) + H → 2H/Fo(001)). The initial 001–O2-Mg1 collapsed to 001–O2-Mg2, the 001–O3-Mg2 complex evolved to 001–O3-Mg1 and 001–Mg1-Mg2 leads to the formation of $H_2$ because the two H atoms are adsorbed on the same Mg atom.

The most stable complexes are those in which one H adsorbs on the Mg atom while the other adsorbs on the O atom, i.e. 001–O1-Mg2, 001–O1-Mg1, 001–O2-Mg2 and 001–O3-Mg1 with calculated $\Delta U_0$ of −110.9, −104.9, −120.0 and −126.8 kcal mol$^{-1}$, respectively. This large stability is due to the formation of both hydride (Mg–H) and an OH group (Si–OH). These complexes are formed because in 001–O1, 001–O2 and 001–O3 cases the unpaired electron is almost entirely localized on the bare Mg atom and, accordingly, prone to receive the second H atom to form Mg–H. Note that for all these diadsorption calculations, the initial guess orbitals corresponded to a broken symmetry solution, which collapsed to a singlet closed shell state. As a consequence, the two hydrogen

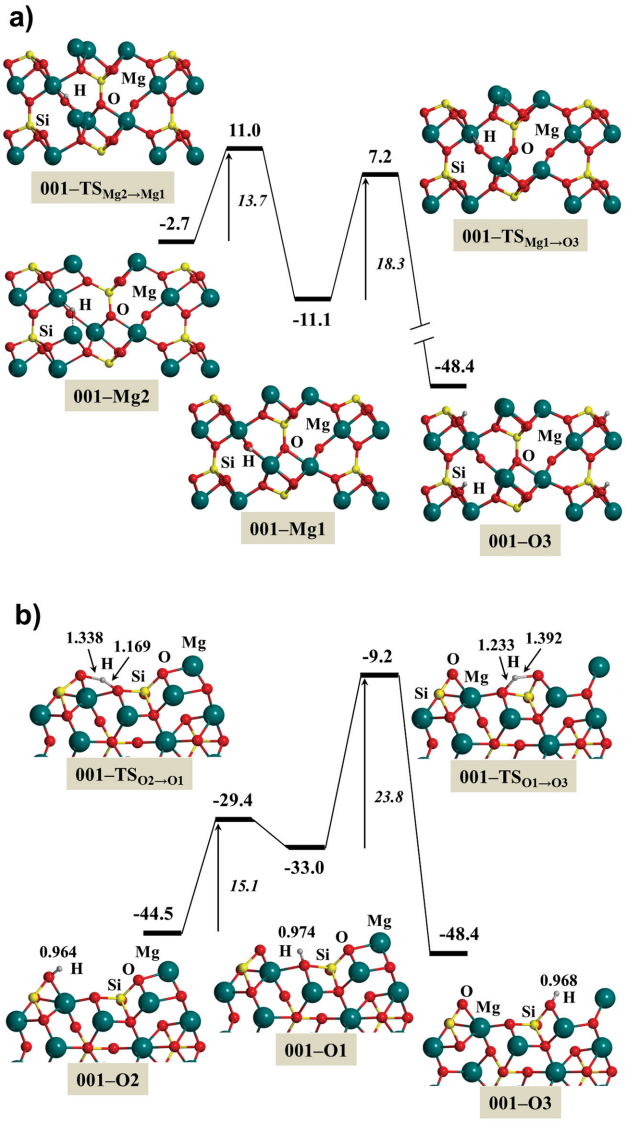


**Figure 3.** B3LYP-D2* energy profiles including ZPE corrections for the inter-conversion between the different adsorption states adopting a 001–Mg2 → 001–Mg1 → 001–O3 (a) and a 001–O2 → 001–O1 → 001–O3 (b) sequence calculated at B2//B1 (bond distances in Å and energies in kcal mol$^{-1}$). Relative energies are referenced with respect to the Fo(001) + H zero-energy asymptote. The unit cell of adducts has been shifted half of the cell parameter *b* to highlight the H-jumps.

atoms become chemisorbed at the surface, the one attached to Mg exhibiting an important hydride character whereas that attached to the oxygen behaving as a proton. Complexes of this kind were also identified in silicate nanoclusters (Kerkeni & Bromley 2013) and in the (010) forsterite surfaces (Goumans et al. 2009; Navarro-Ruiz et al. 2014). The most stable adduct is 001–O3-Mg1 because it also exhibits a dihydrogen bond between the $H^-$ and $H^+$ adatoms, which is confirmed by their Mulliken net charges (−0.35 and +0.35|e|, respectively). The adsorption energies for 001–O2-O1, 001–O3-O1 and 001–O3-O2 are less favourable ($\Delta U_0$ of −62.9, −57.8 and −71.1 kcal mol$^{-1}$, respectively). This lower stability is due to the presence of two silanol (SiOH) groups, which forces the weakening/breaking of different Mg–O bonds. The positive Mulliken net charge of these H atoms (+0.35|e|) is coherent with the formation of an OH group.

*$H_2$ formation.* The interaction of $H_2$ on Fo(001) gives two possible structures (shown in Fig. 2c): one has $H_2$ on the uppermost Mg atom (001–L-$H_2$), and the other on a different and exposed Mg atom belonging to the second edge-layer (001–R-$H_2$). The calculated adsorption energies ($\Delta U_0$ = −3.5 and −2.0 kcal mol$^{-1}$, respectively) indicates that $H_2$ molecule is very weakly bound to Fo(001). Dispersion contribution for both cases is nearly 65 per cent of the adsorption energy. Despite this weak interaction, the reaction energy for the formation of $H_2$ along the Fo(001) + 2H → 001–L-$H_2$ channel is very large and negative (about −107 kcal mol$^{-1}$, see Table 2) because of the release of the $H_2$ formation energy. Nevertheless, the reaction is unfavourable starting from the 001–O3-Mg1 complex (the most stable one), i.e. the 001–O3-Mg1 → 001–L-$H_2$ reaction energy is positive. Table 2 reports the reaction energies for the $H_2$ formation from the 2H/Fo(001) complexes. From these data it results that due to the high stability of 001–O2-Mg2 and 001–O1-Mg2, the $H_2$ formation is an endoergic process. In contrast, the reaction is exoergic when it involves 001–O1-Mg1, 001–O2-O1, 001–O3-O1 and 001–O3-O2 complexes. However, despite the exoergic character of these reactions, they exhibit very high energy barriers, preventing any occurrence of the processes, as they involve the recombination of two H atoms with an $H^+$ character and thus, $H_2$ formation requires an important electronic and structure reorganization. The reaction involving 001–O1-Mg1 implies the recombination of $H^+$ and $H^-$ ions which are too far apart (5.185 Å). Similar situations were already found for the $H_2$ formation on the (010) $Mg_2SiO_4$ surface (Navarro-Ruiz et al. 2014). According to our previous study, the $H_2$ formation is favourable when the two H atoms are either: (i) physisorbed (weakly bound to the surfaces) and couple through a radical–radical process; or (ii) chemisorbed leading to SiOH and Mg–H surface groups in close spatial proximity. For the present (001) surface we did not identify adducts with two physisorbed H atoms, as all cases exhibit chemisorption. The only candidate adduct in which the reaction may exhibit a low-energy barrier is the 001–O3-Mg1 as SiOH and Mg–H groups are in close spatial proximity to make a dihydrogen bond. However, as previously mentioned, this reaction is hampered by unfavourable reaction energy. Therefore, the Langmuir–Hinshelwood recombination of the H adatoms to form an $H_2$ molecule from the doubly H-adsorbed adducts does not seem feasible on the Fo(001) surface.

We also modelled the formation of $H_2$ on the (001) forsterite surface through the Eley–Rideal mechanism by an impinging H atom to the 001–Mg1 adduct. We performed a constrained geometry optimization (a scan calculation), keeping the interatomic H···H distance fixed at specific values (simulating the approach of the incoming H atom) while optimizing the other internal coordinates. The energy variation along the scan calculation shows that the shorter the interatomic distance, the lower the energy of the system, indicating a barrierless process. To confirm this point, we fully relaxed the geometry of the system starting with an initial H···H distance of 3 Å and the system evolved into the spontaneous formation of $H_2$. Thus, provided a high enough H atom flux in the ISM condition, the calculations suggest that the potential energy surface is favourable towards an Eley–Rideal mechanism for the $H_2$ formation on the (001) surface of crystalline forsterite. To better investigate on the feasibility of the Eley–Rideal mechanism, the time-independent quantum reactive scattering calculations to determine the vibrational distributions of product $H_2$ should be carried out. Interestingly, sensible results can already be obtained by limiting the calculation to the bond distance between hydrogen and the surface atom and the intermolecular H···H distance, as Clary and coworkers did for $H_2$ formation on graphite (Farebrother et al.

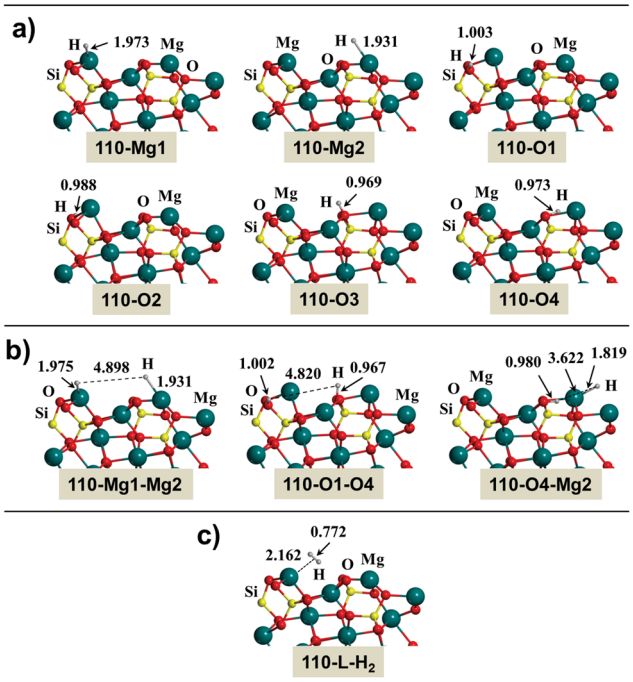


**Figure 4.** B3LYP-D2* optimized geometries of the different complexes on the (110) $Mg_2SiO_4$ surface for the H adsorption (110–Mg1, 110–Mg2, 110–O1, 110–O2, 110–O3 and 110–O4), the different complexes derived from a second H adsorption (110–Mg2-Mg1, 110–O1-O4 and 110–O4-Mg2) and for the adsorption of the most stable $H_2$ conformation (110–L-$H_2$). Bond distances in Å.

2000). They proved that the total reaction probability is very close to 1 for H collision energy compatible to that available at very low temperature of the ISM. Also, the formed $H_2$ molecule leaved the surface in the second excited vibrational level. Due to the similarity with the present system we can roughly assume a similar behaviour also for the forsterite surfaces.

### 3.2.2 *(110) forsterite surface*

*Adsorption of one H atom.* Fig. 4(a) displays the B3LYP-D2*/B1 optimized adducts for the adsorption of one H atom on the Fo(110) slab model and Table 3 reports the B2//B1 calculated adsorption energies. Six different H/Fo(110) adducts were found: two in which the interaction takes place through the outermost Mg atoms (110–Mg1 and 110–Mg2) and four through O atoms (110–O1, 110–O2, 110–O3 and 110–O4), forming the corresponding SiOH surface groups. Physisorption resulted for all the Mg-interacting systems ($\Delta U_0 = -3.8$ and $-5.8$ kcal mol$^{-1}$, respectively, see Table 3), as the major fraction of the spin density is on the H atom (+0.64|e| and +0.61|e|, respectively) and the Mg–H distance (1.973 and 1.931 Å, respectively) is significantly larger than that determined for the chemisorbed 001–Mg1 (1.787 Å) and 001–Mg2 (1.715 Å) species. In contrast, chemisorption dominates the O-interacting systems ($\Delta U_0 = -30.6$, $-26.6$, $-27.4$ and $-41.2$ kcal mol$^{-1}$, respectively) and the spin density basically lies on the adjacent Mg atoms (+0.92|e|, +0.93|e|, +0.91|e| and +0.85|e|, respectively).

Fig. 5(a) shows the energy profile for the 110–Mg2 → 110–O4 path, which goes from the most stable physisorption state to the most stable chemisorption state. The process involves the simultaneous Mg–H breaking/O–H forming bonds. The energy barrier of this H jump is lower than those computed on Fo(001) because here the H atom is physisorbed.

*Adsorption of a second H atom.* For this surface, a total of 15 starting adducts were considered: (i) one from the combination of the two Mg-interacting H/Fo(110) adducts (i.e. 110–Mg1-Mg2); (ii) eight structures derived from the combination of the two Mg-interacting H/Fo(110) with the four O-interacting ones (i.e. 110–O1-Mg1, 110–O1-Mg2, 110–O2-Mg1, 110–O2-Mg2, 110–O3-Mg1, 110–O3-Mg2, 110–O4-Mg1 and 110–O4-Mg2); and (iii) six structures combining the O-interacting H/Fo(110) complexes (i.e. 110–O1-O2, 110–O1-O3, 110–O1-O4, 110–O2-O3, 110–O2-O4 and 110–O3-O4). All the proposed adducts were identified. For the sake of clarity, only the optimized geometry of the most stable adduct for each type of double-adsorption (which are the most relevant ones) are shown in Fig. 4(b) and the corresponding adsorption energies in Table 3. The remaining complexes (both structure and adsorption energies) are reported in ESI.

As occurred for Fo(001), the most stable complex (110–O4-Mg2) ($\Delta U_0 = -120.0$ kcal mol$^{-1}$) has one H adsorbed on a Mg atom and the other on an O atom. In terms of relative stability, this adduct is followed by others in which again the H atoms are simultaneously adsorbed on the Mg and O atoms ($\Delta U_0$ between $-95$ and $-107$ kcal mol$^{-1}$), then by complexes in which the two H atoms are adsorbed on the O atoms ($\Delta U_0$ between $-50$ and $-70$ kcal mol$^{-1}$), and finally by 110–Mg1-Mg2 ($\Delta U_0 = -8.9$ kcal mol$^{-1}$) which is the less stable adduct, as the two H atoms are physisorbed on the two outermost Mg atoms (see ESI).

*$H_2$ formation.* The adsorption of $H_2$ on Fo(110) takes place through the outermost Mg atoms (see 110–L-$H_2$ of Fig. 4c). In the complex, $H_2$ is weakly bound to the surface ($\Delta U_0$ of $-5.1$ kcal mol$^{-1}$), with dispersion contributing to nearly 35 per cent.

Table 3 shows the reaction energies for the formation of $H_2$ from the 2H/Fo(110) complexes shown in Fig. 4(b). The reaction considering 110–O4-Mg2 as the reactant (the most stable adduct) is endoergic, whereas from the other adducts is exoergic. However, from 110–O1-O4, $H_2$ formation implies the recombination of two SiOH protons so that the energy barrier is expected to be significantly high. In contrast, as in 110–Mg1-Mg2 the two H atoms are physisorbed, the reaction is expected to be energetically feasible because it involves a radical–radical coupling. The calculated energy profile is shown in Fig. 5(b) and, unexpectedly, rather than proceeding through a direct H recombination, it involves two steps. In the first step, H jumps from the Mg atom to an O atom, thus forming another and more stable adduct (110–O3-Mg1, already identified as a 2H/Fo(110) complex, see ESI). In the second step, H recombination occurred from the 110–O3-Mg1 structure. The calculated energy barriers were found to be relatively low ($\Delta U_0^{\neq} = 0.4$ and 1.1 kcal mol$^{-1}$ for the first and second steps, respectively).

As done for the Fo(001) surface, we computed the potential energy surface for an Eley–Rideal mechanism by vertically approaching a second H atom to the 110–Mg2 state. At an interatomic H···H distance close to 3.0 Å, the 110–Mg2 adduct spontaneously evolves to the 110–O3 one. In addition, when fully relaxing a system in which the 110–O3 adduct is initially separated by the second H atom by 3.5 Å formation of $H_2$ spontaneously occurred indicating a barrierless process.

## 4 DISCUSSION AND ASTROPHYSICAL IMPLICATIONS

This work is the first quantum chemical study that addresses the adsorption of atomic hydrogen and formation of molecular hydrogen

**Table 3.** B3LYP-D2* reaction energies calculated at the B3LYP-D2*/B2 // B3LYP-D2*/B1 theory level on Fo(110) for: (i) the first H adsorption processes to form 110–Mg1, 110–Mg2, 110–O1, 110–O2, 110–O3 and 110–O4 adducts; (ii) the global H adsorption processes to form the 110–Mg1-Mg2, 110–O1-O4, 110–O4-Mg2 and 110–L-$H_2$ complexes and (iii) the $H_2$ formation from the 2H/Fo(110) complexes. The zero-energy reference is the Fo(110) + H asymptote. Uncorrected ($\Delta E$) and ZPE-corrected ($\Delta U_0$) adsorption energy. Bare values in kcal mol$^{-1}$, in parenthesis in meV, in brackets in K.

| Reaction | $\Delta E$ | | | $\Delta U_0$ | | |
|---|---|---|---|---|---|---|
| Fo(110) + H → 110–Mg1 | − 6.0 | (−262) | [−3036] | − 3.8 | (−165) | [−1913] |
| Fo(110) + H → 110–Mg2 | − 7.9 | (−342) | [−3966] | − 5.8 | (−252) | [−2929] |
| Fo(110) + H → 110–O1 | − 37.0 | (−1604) | [−18 610] | − 30.6 | (−1327) | [−15 402] |
| Fo(110) + H → 110–O2 | − 33.0 | (−1432) | [−16 620] | − 26.6 | (−1154) | [−13 386] |
| Fo(110) + H → 110–O3 | − 34.0 | (−1475) | [−17 117] | − 27.4 | (−1189) | [−13 800] |
| Fo(110) + H → 110–O4 | − 47.7 | (−2068) | [−23 996] | − 41.2 | (−1786) | [−20 726] |
| Fo(110) + 2H → 110–Mg1-Mg2 | − 13.2 | (−574) | [−6661] | − 8.9 | (−387) | [−4496] |
| Fo(110) + 2H → 110–O1-O4 | − 82.5 | (−3575) | [−41 492] | − 69.8 | (−3025) | [−35 105] |
| Fo(110) + 2H → 110–O4-Mg2 | − 130.7 | (−5669) | [−65 785] | − 120.0 | (−5206) | [−60 411] |
| Fo(110) + 2H → 110–L-$H_2$ | − 118.4 | (−5133) | [−59 570] | − 108.8 | (−4720) | [−54 770] |
| 110–Mg1-Mg2 → 110–L-$H_2$ | − 105.2 | (−4559) | [−52 909] | − 99.9 | (−4332) | [−50 275] |
| 110–O1-O4 → 110–L-$H_2$ | − 35.9 | (−1558) | [−18 078] | − 39.1 | (−1694) | [−19 665] |
| 110–O4-Mg2 → 110–L-$H_2$ | 12.4 | (536) | [6215] | 11.2 | (486) | [5641] |

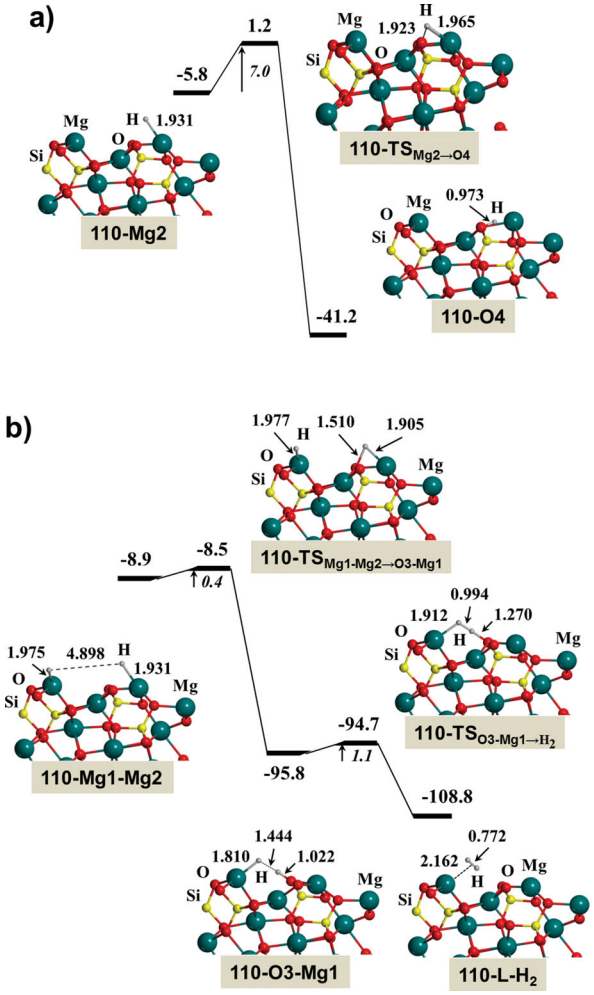


**Figure 5.** B3LYP-D2* energy profiles including ZPE corrections for the 110–Mg2 → 110–O4 inter-conversion path (a) and the recombination of two H atoms to form $H_2$ on the (110) $Mg_2SiO_4$ surface (b) calculated at B2//B1 (bond distances in Å and energies in kcal mol$^{-1}$). Relative energies are referenced with respect to the Fo(110) + H and Fo(110) + 2H zero-energy asymptote, respectively.

on the (001) and (110) surfaces of crystalline forsterite. These surfaces have higher surface energy (1.67 and 1.79 J m$^{-2}$, respectively) than the most stable (010) one (1.16 J m$^{-2}$) studied recently by us (Navarro-Ruiz et al. 2014), giving insights on the role of crystal morphology on $H_2$ formation.

A first interesting datum is that, compared to the (010) surface, the (001) and (110) surfaces are more heterogeneous, exhibiting a higher number of potential adsorption sites, which have all been addressed here. Quite obviously, the more negative the H adsorption energy, the higher the associated surface energy, thus showing a clear correlation. This is shown by the adsorption energy of the most stable singly H chemisorbed adducts on the (010), (001) and (110) faces (−10.3, −48.4 and −41.2 kcal mol$^{-1}$, respectively) which are in line with the surface energy values. This also affects the diffusion behaviour of H atoms on these surfaces. H jumps on the (010) surface exhibit lower energy barriers (between 4 and 6 kcal mol$^{-1}$) compared to those on the (001) and (110) surfaces (between 7 and 23 kcal mol$^{-1}$).

The different adsorption features between these $Mg_2SiO_4$ surfaces also have significant consequences on the H recombination to form $H_2$ through a Langmuir–Hinshelwood mechanism. On the (010) surface, two paths were identified as feasible (Navarro-Ruiz et al. 2014), one based on a radical–radical H coupling and the other on an $H^+\cdots H^-$ recombination. In contrast, on the (001) surface, all reaction channels resulted to be energetically unfavourable, because the 2H/Fo(001) initial states are more stable than the $H_2$/Fo(001) final product, whereas for the (110) surface, only one favourable channel ($H^+\cdots H^-$ recombination) leading to the formation of $H_2$ has been elucidated. These results indicate that the larger instability of the (001) and (110) surfaces makes them very reactive towards H adsorption, with the consequence that the high stability of the formed complexes inhibits the formation of $H_2$. Investigation on the potential energy surface of H impinging on hydrogen pre-adsorbed on the (001) and (110) surfaces suggest that the Eley–Rideal mechanism may become important due to the barrierless nature of the process. However, the low H density in diffuse clouds of the ISM decreases the probability of the Eley–Rideal mechanism and, consequently, the present results suggest that among these three crystalline faces, the (010) is the most active one as far as $H_2$ formation is concerned, through a Langmuir–Hinshelwood mechanism.

**Table 4.** B3LYP-D2* ZPE-corrected energy barriers ($\Delta U_0^{\neq}$, in kcal mol$^{-1}$) at the B2//B1 level, transition frequencies ($\nu^{\neq}$, in cm$^{-1}$) and tunnelling crossover temperatures ($T_X$, in K).

| Reaction | $\Delta U_0^{\neq}$ | $\nu^{\neq}$ | $T_X$ |
|---|---|---|---|
| Fig. 3 | | | |
| (a) 001–Mg2 → 001–Mg1 | 13.7 | 249 | 57 |
| (a) 001–Mg1 → 001–O3 | 18.3 | 946 | 220 |
| (b) 001–O2 → 001–O1 | 15.1 | 1048 | 245 |
| (b) 001–O1 → 001–O3 | 23.8 | 1560 | 365 |
| Fig. 5 | | | |
| (a) 110–Mg2 → 110–O4 | 7.0 | 500 | 117 |
| (b) 110–Mg1-Mg2 → 110–O3-Mg1 | 0.4 | 626 | 278 |
| (b) 110–O3-Mg1 → 110–L-$H_2$ | 1.1 | 761 | 220 |
| Fo(010)[a] | | | |
| P1 → P2 | 4.1 | 137 | 32 |
| P2 → C1 | 6.4 | 1058 | 264 |
| P2–P2 → Fo–$H_2$ | 0.5 | 361 | 108 |
| C1–P2b → Fo–$H_2$ | 1.7 | 1110 | 320 |

*Note*. [a]Taken from Navarro-Ruiz et al. (2014).

Finally, we have examined the trend of the kinetics of the different H hoping and H recombination on the (010), (001) and (110) surfaces. To this end, we calculated the crossover temperature ($T_X$) for each surface process and using equations (3)–(5) we represented the Arrhenius plots of $k^{SC\text{-}TST}$ in which above $T_X$ we considered $\Gamma(T) = 1$. Calculated $T_X$ values, alongside the values of $\Delta U_0^{\neq}$ and $\nu^{\neq}$ used, are shown in Table 4, and the Arrhenius plots are represented in Fig. 6. It is worth mentioning that as the employed $\Gamma(T)$ expression is stable to arbitrarily low temperatures, the Arrhenius plots were represented between 150 and 450 K. We have not considered lower temperatures because this will require more accurate treatments of tunnelling effects such as Feynman's path integral formalisms, as already done in H-based processes on carbonaceous surfaces (Goumans & Kästner 2010; Goumans 2011). On the (001) surface (Fig. 6a), tunnelling contributions are expected to be significant in the range of the considered temperatures for the 001–Mg1 → 001–O3, 001–O2 → 001–O1 and 001–O1 → 001–O3 H hopping because the corresponding Arrhenius plots show a prominent slope change, which makes $\log_{10}(k^{SC\text{-}TST})$ values to remain relatively constant below $T_X$ as occurs in regimes dominated by tunnelling. This is at variance with the 001–Mg2 → 001–Mg1 path ($T_X = 57$ K) because it is not strictly an H jump but a Mg–O breaking followed by an H rearrangement on the Mg atom. However, the calculated $\log_{10}(k^{SC\text{-}TST})$ values are small at the low-temperature range (between 0 and −5 at 150 K), pointing out that these H jumps are kinetically hindered at the interstellar temperatures. For processes on the (110) surface (Fig. 6b), it is found that the $T_X$ for the 110–Mg2 → 110–O4 H hopping is about 120 K and accordingly no slope change is observed in our Arrhenius plot. For the processes involved in the $H_2$ formation (i.e. 110–Mg1-Mg2 → 110–O3-Mg2 and 110–O3-Mg1 → 110–L-$H_2$), although the calculated $T_X$ are above 100 K (278 and 220 K, respectively), no considerable slope changes are observed, meaning that, regardless of tunnelling contributions, the $H_2$ formation reaction is fast (the calculated $\log_{10}(k^{SC\text{-}TST})$ are above 12.5 at the range of temperatures) because the corresponding energy barriers are very low ($\Delta U_0^{\neq} = 0.4$ and 1.2 kcal mol$^{-1}$, respectively). Finally, on the (010) surface (Fig. 6c), neither the P1 → P2 H hopping nor the P2–P2 → Fo–$H_2$ $H_2$ formation (namely, those processes involving exclusively physisorbed H atoms) are affected by tunnelling, whose calculated

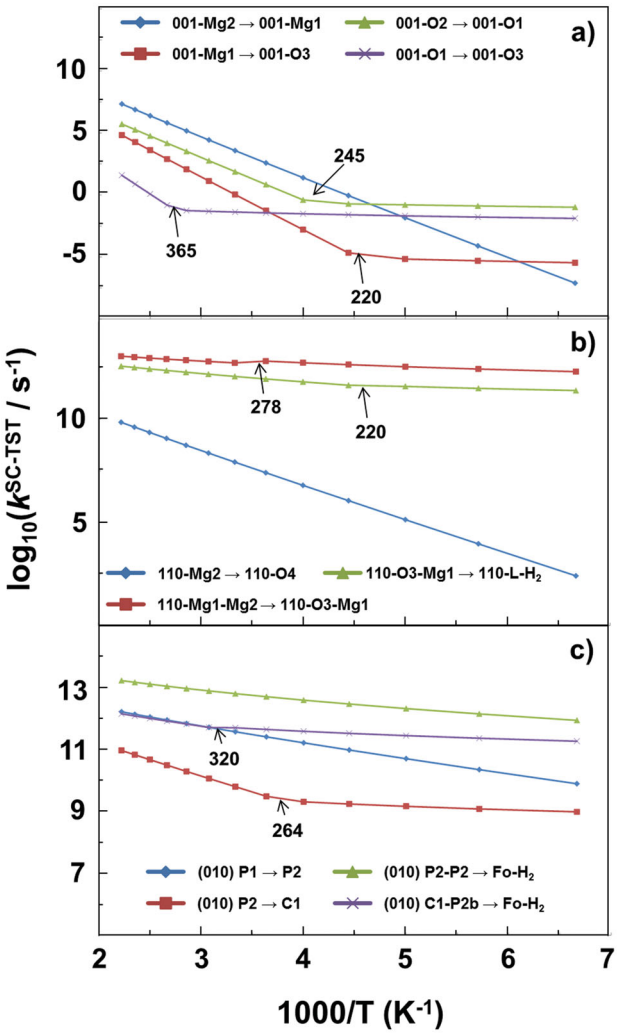


**Figure 6.** Arrhenius plots of $k^{SC\text{-}TST}$ between 150 and 450 K. Crossover temperatures ($T_X$) are indicated for each process on the (001) (a), (110) (b) and (010) (c) surfaces. Above $T_X$ we considered $\Gamma(T) = 1$.

$T_X$ values are 32 and 108 K, respectively. Both processes are fast at the range of temperatures since the calculated $\log_{10}(k^{SC\text{-}TST})$ values are about 11 and 13, respectively, at 150 K. For the P2 → C1 H hopping (namely, the change of a physisorbed into a chemisorbed H atom) tunnelling effects seem to be significant due to the slope change at its crossover temperature ($T_X = 264$ K), whereas for the C1-P2b → Fo–$H_2$ $H_2$ formation (namely, the coupling involving an $H^+ \cdots H^-$ recombination) a small but appreciable slope change takes place at its crossover temperature ($T_X = 320$ K), in which, moreover, the calculated $\log_{10}(k^{SC\text{-}TST})$ values indicate that the processes are fast (about 9 and 12, respectively, at 150 K).

## 5 CONCLUSIONS

In this work the crystalline (001) and (110) surfaces of $Mg_2SiO_4$ forsterite have been used as models for the core of the interstellar dust particle using a quantum mechanical approach based on periodic density functional calculations. The adsorption of atomic hydrogen and the formation of molecular hydrogen has been studied in detail using the B3LYP-D2* method combined with flexible

polarized Gaussian-type basis sets, which allows a balanced description of the H/surface interactions for both minima and activated complexes. As these two faces are more unstable than the (010) most stable one, comparison of the results between these three surfaces has been addressed.

The different adsorption states envisage chemisorption occurring both on the Mg and on the O atoms. Hydrogen physisorption occurs essentially on the Mg atoms. The calculated adsorption energies for the chemisorption states are large and significantly stronger than the (010) surface. The calculated energy profiles on the (001) and (110) faces indicate that the H jumps through different adsorption states are energetically more expensive in most of the calculated paths than on the (010) one due to the large hydrogen/surface interactions.

The most stable doubly H adsorbed complexes are those in which Mg–H and SiO–H surface groups are formed. On the most stable (010) surface, the H recombination processes to give $H_2$ from the doubly H adsorbed complexes occurs through a Langmuir–Hinshelwood mechanism. In contrast, on the (001) surface the process is endoergic because of the larger stability of the initial states, causing the final products to be more unstable. The (110) surface exhibits an intermediate character, as only one reactive channel leading to $H_2$ formation is energetically feasible at ISM conditions. The associated potential energy surface for the Eley–Rideal mechanism, in which an H atom impinges on an H pre-adsorbed forsterite surface, has also been computed. Due to the barrierless process occurring in these cases, the Eley–Rideal mechanism is expected to be efficient also at very low H collision energy estimated for the low temperature of the ISM region. Low H atom flux is nevertheless the most limiting factor for this mechanism to become relevant in the ISM.

Finally, represented Arrhenius plots between 150 and 450 K indicate that, at this range of temperatures, the H hopping processes on the (001) surfaces are kinetically hindered at low temperatures although tunnelling effects are predicted to be significant, whereas on the (110) surface, those processes involved in the $H_2$ formation are found to be fast irrespective of tunnelling contributions, and on the (010) surface, all the processes are fast, in which related to $H_2$ formation, the radical–radical H coupling does not exhibit tunnelling dependence, whereas the $H^+ \cdots H^-$ recombination tunnelling effects allow this reaction to be fast at low temperatures.

## ACKNOWLEDGEMENTS

Financial support from MICINN (projects CTQ2011–24847/BQU, CTQ2014–59544-P, CTQ2013–40347-ERC and CTQ2014–60119-P) and DIUE (project 2014SGR482) is gratefully acknowledged. JN-R is indebted to SUR of ECO of Generalitat de Catalunya for a predoctoral grant. AR is indebted to Programa Banco de Santander for a UAB distinguished postdoctoral research contract. MS gratefully acknowledges support through 2011 ICREA Award. PU acknowledges Progetti di Ricerca di Ateneo-Compagnia di San Paolo-2011-Linea 1A, progetto ORTO11RRT5 for funding. AR kindly acknowledges BSC-MN for the generous allowance of computing time through the 'QCM-2013–2–0006: Formation of Molecular Hydrogen on Surfaces of Cosmic Dust', 'QCM-2013–3–0015: Adsorption of Atomic Hydrogen on Defective Non-Stoichiometric Surfaces of Cosmic Dust' and 'QCM-2014–3–0032: Quantum Effects in the Diffusion of Atomic Hydrogen on Interstellar Silicate Surfaces' projects. The use of the Catalonia Supercomputer Centre (CESCA) is gratefully acknowledged.

## REFERENCES

Bachellerie D., Sizun M., Aguillon F., Teillet-Billy D., Rougeau N., Sidis V., 2009, Phys. Chem. Chem. Phys., 11, 2715
Baouche S., Gamborg G., Petrunin V. V., Luntz A. C., Baurichter A., Hornekær L., 2006, J. Chem. Phys., 125, 084712
Becke A. D., 1993, J. Chem. Phys., 98, 5648
Boese A. D., Sauer J., 2013, Phys. Chem. Chem. Phys., 15, 16481
Bruno M., Massaro F. R., Prencipe M., Demichelis R., De La Pierre M., Nestola F., 2014, J. Phys. Chem. C, 118, 2498
Casolo S., Tantardini G. F., Martinazzo R., 2013, Proc. Natl. Acad. Sci., 110, 6674
Cazaux S., Tielens A. G. G. M., 2004, ApJ, 604, 222
Civalleri B., D'Arco P., Orlando R., Saunders V. R., Dovesi R., 2001, Chem. Phys. Lett., 348, 131
Civalleri B., Zicovich-Wilson C. M., Valenzano L., Ugliengo P., 2008, CrystEngComm, 10, 405
Civalleri B., Maschio L., Ugliengo P., Zicovich-Wilson C. M., 2010, Phys. Chem. Chem. Phys., 12, 6382
Creighan S. C., Perry J. S. A., Price S. D., 2006, J. Chem. Phys., 124, 114701
de Leeuw N. H., Parker S. C., Catlow C. R. A., Price G. D., 2000, Phys. Chem. Miner., 27, 332
Doll K., 2001, Comput. Phys. Comm., 137, 74
Dovesi R., Orlando R., Civalleri B., Roetti C., Saunders V. R., Zicovich-Wilson C. M., 2005, Z. Kristallogr., 220, 571
Dovesi R. et al., 2009, CRYSTAL09 User's Manual. Univ. Torino, Torino
Downing C. A., Ahmady B., Catlow C. R. A., de Leeuw N. H., 2013, Phil. T. R. Soc. A, 371, 20110592
Draine B. T., 2003, ARA&A, 41, 241
Duley W. W., Williams D. A., 1993, MNRAS, 260, 37
Dyson J. E., Williams D. A., 1997, The Physics of the Interstellar Medium. Taylor & Francis, New York
Eley D. D., 1941, P. R. Soc. A, 178, 452
Eley D. D., Rideal E. K., 1940, Nature, 146, 401
Farebrother A. J., Meijer A. J. H. M., Clary D. C., Fisher A. J., 2000, Chem. Phys. Lett., 319, 303
Fermann J. T., Auerbach S., 2000, J. Chem. Phys., 112, 6787
Garcia-Gil S., Teillet-Billy D., Rougeau N., Sidis V., 2013, J. Phys. Chem. C, 117, 12612
Gould R. J., Salpeter E. E., 1963, ApJ, 138, 393
Goumans T. P. M., 2011, MNRAS, 415, 3129
Goumans T. P. M., Bromley S. T., 2011, MNRAS, 414, 1285
Goumans T. P. M., Kästner J., 2010, Angew. Chem. Int. Ed., 49, 7350
Goumans T. P. M., Catlow C. R. A., Brown W. A., 2009, MNRAS, 393, 1403
Grimme S., 2006, J. Comput. Chem., 27, 1787
Harris J., Kasemo B., 1981, Surf. Sci., 105, L281
He J., Frank P., Vidali G., 2011, Phys. Chem. Chem. Phys., 13, 15803
Henning T., 2010, ARA&A, 48, 21
Herbst E., Chang Q., Cuppen H. M., 2005, J. Phys. Conf. Ser., 6, 18
Hinshelwood C. N., 1930, Annu. Rep. Prog. Chem., 27, 11
Hornekær L., Baurichter A., Petrunin V. V., Field D., Luntz A. C., 2003, Science, 302, 1943
Hornekær L. et al., 2006, Phys. Rev. Lett., 96, 156104
Islam F., Latimer E. R., Price S. D., 2007, J. Chem. Phys., 127, 064701
Katz N., Furman I., Biham O., Pirronello V., Vidali G., 1999, ApJ, 522, 305
Kerkeni B., Bromley S. T., 2013, MNRAS, 435, 1486
Langmuir I., 1922, Trans. Faraday Soc., 17, 621
Latimer E. R., Islam F., Price S. D., 2008, Chem. Phys. Lett., 455, 174
Latter W. B., Black J. H., 1991, ApJ, 372, 161
Meijer A. J. H. M., Fisher A. J., Clary D. C., 2003, J. Phys. Chem. A, 107, 10862
Molster F., Kemper C., 2005, Space Sci. Rev., 119, 3
Morisset S., Aguillon F., Sizun M., Sidis V., 2005, J. Chem. Phys., 122, 194702
Navarro-Ruiz J., Sodupe M., Ugliengo P., Rimola A., 2014, Phys. Chem. Chem. Phys., 16, 17447

Pascale F., Zicovich-Wilson C. M., López Gejo F., Civalleri B., Orlando R., Dovesi R., 2004, J. Comput. Chem., 25, 888
Perets H. B., Biham O., Manicó G., Pirronello V., Roser J., Swords S., Vidali G., 2005, ApJ, 627, 850
Perets H.B. et al., 2007, ApJ, 661, L163
Pirronello V., Biham O., Liu C., Shen L., Vidali G., 1997, ApJ, 483, L131
Rimola A., Zicovich-Wilson C. M., Dovesi R., Ugliengo P., 2010, J. Chem. Theory Comput., 6, 1341
Rougeau N., Teillet-Billy D., Sidis V., 2011, Phys. Chem. Chem. Phys., 13, 17579
Schafer A., Horn H., Ahlrichs R., 1992, J. Chem. Phys., 97, 2571
Tielens A.G.G.M., 2005, The Physics and Chemistry of the Interstellar Medium. Cambridge Univ. Press, Cambridge
Ugliengo P., Damin A., 2002, Chem. Phys. Lett., 366, 683
Vidali G., 2013, Chem. Rev., 113, 8762
Vidali G., Roser J. E., Ling L., Congiu E., Manico G., Pirronello V., 2006, Faraday Discuss., 133, 125
Vidali G. et al., 2007, J. Phys. Chem. A, 111, 12611
Watson G. W., Oliver P. M., Parker S. C., 1997, Phys. Chem. Miner., 25, 70

## SUPPORTING INFORMATION

Additional Supporting Information may be found in the online version of this article:

**Figure A1.** B3LYP-D2* optimized geometries of the complexes exhibiting two H atoms or the $H_2$ molecules adsorbed on the (110) slab models. Bond distances are in Å.
**Table A1.** Net charges and electronic spin densities computed at B2//B1 level for the different H/Fo adducts.
**Table A2.** Computed adsorption energies of one H atom on Fo(001) for the different 001–Mg1, 001–Mg2, 001–O1, 001–O2 and 001–O3 adducts at the B3LYP-D2*/B1 and B3LYP-D2*/B2//B3LYP-D2*/B1 levels of theory. B3LYP adsorption energy ($\Delta E_{el}$); contribution of dispersion to the adsorption energy ($\Delta E_{D2^*}$); B3LYP-D2* adsorption energy ($\Delta E = \Delta E_{el} + \Delta E_{D2^*}$); and ZPE-corrected adsorption energy ($\Delta U_0 = \Delta E + \Delta E_0$). Bare values in kcal mol$^{-1}$, in parenthesis in meV, in brackets in K.
**Table A3.** B3LYP-D2* reaction energies calculated at B1 and B2//B1 levels for the adsorption of a second H atom on all the H/Fo(001) complexes. Uncorrected ($\Delta E$) and ZPE-corrected ($\Delta U_0$) adsorption energies. Bare values in kcal mol$^{-1}$, in parenthesis in meV, in brackets in K.
**Table A4.** B3LYP-D2* reaction energies calculated at B1 and B2//B1 levels for the global H adsorption processes on Fo(001) to form the 001–O1-Mg2, 001–O1-Mg1, 001–O2-Mg2, 001–O3-Mg1, 001–O2-O1, 001–O3-O1, 001–O3-O2, 110–L-$H_2$ and 110–R-$H_2$ complexes. Uncorrected ($\Delta E$) and ZPE-corrected ($\Delta U_0$) adsorption energies. Bare values in kcal mol$^{-1}$, in parenthesis in meV, in brackets in K.
**Table A5.** B3LYP-D2* reaction energies calculated at B1 and B2//B1 levels for the $H_2$ formation from the 2H/Fo(001) complexes. Uncorrected ($\Delta E$) and ZPE-corrected ($\Delta U_0$) adsorption energies. Bare values in kcal mol$^{-1}$, in parenthesis in meV, in brackets in K.
**Table A6.** B3LYP-D2* adsorption energies calculated at B1 and B2//B1 levels of $H_2$ molecule on the Fo(001) and Fo(110) surface slab models. Uncorrected ($\Delta E$) and ZPE-corrected ($\Delta U_0$) adsorption energies. Bare values in kcal mol$^{-1}$, in parenthesis in meV, in brackets in K.
**Table A7.** Computed adsorption energies of one H atom on the (110) slab models for the different 110–Mg1, 110–Mg2, 110–O1, 110–O2, 110–O3 and 110–O4 adducts at the B3LYP-D2*/B1 and B3LYP-D2*/B2 // B3LYP-D2*/B1 levels of theory. The zero-energy reference is the Fo(110) + H asymptote. B3LYP adsorption energy ($\Delta E_{el}$); contribution of dispersion to the adsorption energy ($\Delta E_{D2^*}$); B3LYP-D2* adsorption energy ($\Delta E = \Delta E_{el} + \Delta E_{D2^*}$); and ZPE-corrected adsorption energy ($\Delta U_0 = \Delta E + \Delta E_0$). Bare values in kcal mol$^{-1}$, in parenthesis in meV, in brackets in K.
**Table A8.** B3LYP-D2* reaction energies calculated at B1 and B2//B1 levels for the adsorption of a second H atom on the H/Fo(110) complexes. Uncorrected ($\Delta E$) and ZPE-corrected ($\Delta U_0$) adsorption energies. Bare values in kcal mol$^{-1}$, in parenthesis in meV, in brackets in K.
**Table A9.** B3LYP-D2* reaction energies calculated at B1 and B2//B1 levels for the global H adsorption processes on the (110) slab models. Uncorrected ($\Delta E$) and ZPE-corrected ($\Delta U_0$) adsorption energies. Bare values in kcal mol$^{-1}$, in parenthesis in meV, in brackets in K.
**Table A10.** B3LYP-D2* reaction energies calculated at B1 and B2//B1 levels for the $H_2$ formation from the 2H/Fo(110) complexes. Uncorrected ($\Delta E$) and ZPE-corrected ($\Delta U_0$) adsorption energies. Bare values in kcal mol$^{-1}$, in parenthesis in meV, in brackets in K (http://mnras.oxfordjournals.org/lookup/suppl/doi:10.1093/mnras/stv1628/-/DC1).

Please note: Oxford University Press are not responsible for the content or functionality of any supporting materials supplied by the authors. Any queries (other than missing material) should be directed to the corresponding author for the article.

This paper has been typeset from a TEX/LATEX file prepared by the author.